Exploring Relativistic Many-Body Recoil Effects in Highly Charged Ions

R. Soria Orts,[1] Z. Harman,[1] J. R. Crespo López-Urrutia,[1] A. N. Artemyev,[1,2] H. Bruhns,[1] A. J. González Martínez,[1] U. D. Jentschura,[1] C. H. Keitel,[1] A. Lapierre,[1] V. Mironov,[1] V. M. Shabaev,[2] H. Tawara,[1] I. I. Tupitsyn,[1,2] J. Ullrich,[1] and A. V. Volotka[2]

[1]*Max-Planck-Institut für Kernphysik, Saupfercheckweg 1, 69117 Heidelberg, Germany*

[2]*Department of Physics, St. Petersburg State University, Oulianovskaya 1, Petrodvorets, St. Petersburg 198504, Russia*

(Received 2 June 2006; published 6 September 2006)

The relativistic recoil effect has been the object of experimental investigations using highly charged ions at the Heidelberg electron beam ion trap. Its scaling with the nuclear charge Z boosts its contribution to a measurable level in the magnetic-dipole ($M1$) transitions of B- and Be-like Ar ions. The isotope shifts of ^{36}Ar versus ^{40}Ar have been detected with sub-ppm accuracy, and the recoil effect contribution was extracted from the $1s^2 2s^2 2p\ ^2P_{1/2} - {}^2P_{3/2}$ transition in Ar^{13+} and the $1s^2 2s 2p\ ^3P_1 - {}^3P_2$ transition in Ar^{14+}. The experimental isotope shifts of 0.00123(6) nm (Ar^{13+}) and 0.00120(10) nm (Ar^{14+}) are in agreement with our present predictions of 0.00123(5) nm (Ar^{13+}) and 0.00122(5) nm (Ar^{14+}) based on the total relativistic recoil operator, confirming that a thorough understanding of correlated relativistic electron dynamics is necessary even in a region of intermediate nuclear charges.

DOI: 10.1103/PhysRevLett.97.103002 PACS numbers: 31.30.Jv, 32.10.Bi, 32.70.Jz

Traditionally, measurements of optical isotope shifts in atomic spectra have been carried out mainly to determine changes in the mean square nuclear charge radii $\langle r^2 \rangle$, among other nuclear properties affecting the atomic structure. More recently, new applications have emphasized the relevance of this field. For instance, isotope shift calculations in atoms and ions with one valence electron above closed shells can help explain the spectral line shifts observed in quasar absorption spectra that had otherwise suggested a variation of the fine-structure constant [1,2].

Although the study of these effects in highly charged ions (HCI) has the potential advantage of an increased sensitivity to nuclear size and relativistic effects, only a few of the spectroscopic measurements with HCI offer sufficient accuracy for meaningful studies. The advantage of studying HCI is a consequence of the stronger overlap of the electronic wave function with the nuclear matter and of the simpler electronic structure of few-electron ions as opposed to their neutral atomic counterparts. The latter reason is indeed very important, since the theoretical treatment of electron correlation is still the largest source of uncertainties in the analysis of heavy-ion experiments aiming at a determination of physical properties of the nucleus or of its constituents, as is the case for parity nonconservation experiments [3,4], among others.

An investigation of mass shifts of ground state magnetic-dipole transitions in few-electron ions of medium nuclear charge combines two aspects of atomic physics: (i) the correlated relativistic many-electron problem, and (ii) relativistic contributions to the nuclear recoil operator. The latter can only be obtained via a full quantum electrodynamic (QED) formulation of the problem [5]. The measurement can provide stringent tests of the QED theory of many-body systems, and thereby recent progress is being extended to higher nuclear charge numbers. In recent experiments, the charge radii of light halo nuclei have been determined by laser spectroscopy combined with very accurate theoretical work [for ^{6}He, see Ref. [6], and for ^{8,9}Li, see Ref. [7]]. Enhanced systematic studies of nuclear properties seem possible nowadays using atomic-physics techniques in view of the advances in experimental facilities (e.g., electron beam ion traps, EBITs) on the one side and in the atomic theory on the other side.

Isotope shifts arise from the combined effect of the finite nuclear mass and volume on the electronic binding energy. The mass-dependent, or recoil part, is usually divided into the so-called normal mass shift and the specific mass shift (mass polarization). In HCI, large relativistic nuclear recoil contributions must be included. The volume effect, also called the field shift (FS), is caused by the penetration of the electronic wave function into the nucleus. Its magnitude grows roughly with the sixth power of Z and becomes comparable to that of the QED contributions for the heaviest elements.

An application of the nonrelativistic theory of recoil effects in many-body problems can be found in, e.g., Ref. [8]. Relativistic corrections to the recoil operator are discussed in detail in Ref. [9]. The many-body relativistic recoil operator for a general atomic system of electrons with indices i, j, reads [see Refs. [5,10], in relativistic units, $\hbar = c = \epsilon_0 = 1$]

$$R_{ij} = \frac{\boldsymbol{p}_i \cdot \boldsymbol{p}_j}{2M} - \frac{Z\alpha}{2Mr_i}\left(\boldsymbol{\alpha}_i + \frac{(\boldsymbol{\alpha}_i \cdot \boldsymbol{r}_i)\boldsymbol{r}_i}{r_i^2}\right) \cdot \boldsymbol{p}_j. \quad (1)$$

Here, $\boldsymbol{r}_i$ and $\boldsymbol{p}_i$ are the position vector and the momentum operator of the ith electron, respectively, and $\boldsymbol{\alpha}_i$ is the vector of Dirac matrices acting on its bispinor wave function. The isotope-dependent nuclear mass is denoted by M and α is the fine-structure constant. The normal mass shift correction to a given atomic state is obtained as the expectation value $\langle \sum_i R_{ii} \rangle$, whereas the specific mass shift term is

given by $\langle \sum_{i \neq j} R_{ij} \rangle$. The first term in Eq. (1) corresponds to the mass shift operator also known in the nonrelativistic theory. The evidently large effect of the relativistic operator corrections in Ar^{13+} and Ar^{14+} is illustrated in Table I, which represents a breakdown of the normal and specific mass shifts [first term in Eq. (1), denoted by NMS and SMS], relativistic operator contributions [second term in Eq. (1), denoted by RNMS and RSMS]. We would like to stress that since expectation values of the NMS and SMS operators are evaluated with Dirac wave functions, the entries denoted by NMS and SMS in Table I contain a part of the relativistic contributions. As we consider transitions between fine-structure components, the nonrelativistic recoil contribution is equal to zero. Furthermore, in our systems, the mass shift terms strongly dominate over the FS.

The NMS, SMS, RNMS, and RSMS contributions in Table I completely define the nuclear recoil corrections within the $(\alpha Z)^4 m_e^2/M$ approximation (m_e denotes the mass of the electron) and can be derived from the Breit equation. The contributions denoted by QED require using QED beyond the Breit approximation [5,11].

In the present work, we investigate the ^{36}Ar–^{40}Ar isotope shift of the $M1$ transitions $1s^2 2s^2 2p\ ^2P_{1/2} - {}^2P_{3/2}$ in Ar^{13+} and the $1s^2 2s 2p\ ^3P_1 - {}^3P_2$ in Ar^{14+}, whose wavelengths (for ^{40}Ar) have recently been determined to be 441.2559(1) and 594.3880(5) nm, respectively [12]. The experiments were performed using the electron beam ion trap at the Max-Planck-Institut für Kernphysik.

The ions contained in an EBIT are produced by an intense electron beam, highly compressed by an axial magnetic field of 8 T. The beam also keeps the ions radially trapped within a cloud of roughly 0.1 mm diameter. Several appropriately biased drift tubes confine the axial ion motion to within a length of 40 mm [13]. Trapping times of seconds to hours and electron current densities of the order of $10^{22} e\ \mathrm{s}^{-1}\ \mathrm{cm}^{-2}$ lead to the production of ions in average charge states with electronic binding energies for the remaining bound electrons just slightly lower than the electron beam energy. The electron beam energy and current chosen for this experiment are $E_{\mathrm{beam}} = 0.8$–1.1 keV and $I_e = 10$–90 mA, respectively.

TABLE I. Relativistic recoil operator and QED contributions to the mass shift and field shift (^{36}Ar–^{40}Ar) in Ar^{13+} and Ar^{14+} ions (in cm^{-1}). See text for explanations.

	Ar^{13+}	Ar^{14+}
NMS	0.1052	0.0796
RNMS	−0.0822	−0.0627
One-electron QED	0.0002	0.0002
SMS	−0.0741	−0.0697
RSMS	0.1151	0.0887
Two-electron QED	−0.0008	−0.0015
FS	−0.0005	−0.0001
Sum	0.0629	0.0345

The technique of evaporative cooling was applied in order to lower the translational temperature T_{ion} of the trapped ions from values typically found at EBITs of several hundred eV down to only $T_{\mathrm{ion}} \approx 6$ eV, the lowest temperature reported in such a trap to the best of our knowledge. The cooling was achieved by intentionally reducing both the axial trapping voltage [14] and the electron beam current, resulting in the evaporation of hot ions. A considerable decrease of the spectral width of the emission lines and, by consequence, the Zeeman splitting, could be clearly observed (see Fig. 1).

A low-density, collimated atomic beam either from ^{40}Ar (99.998% pure) or ^{36}Ar (99.7% pure) samples was injected into the trap. Before switching from ^{36}Ar to ^{40}Ar, the gas injection system was carefully pumped out and purged to avoid isotopic contamination. By extracting ions from the trap and measuring their q/m (charge/mass) ratio distributions with an analyzing magnet, their isotopic composition was also tested.

A real image of the ion cloud was projected by *in-vacuo* lenses through a quartz window onto the outside of the vacuum chamber, and further relayed by external lenses to the entrance slit of a 0.6 m focal length Czerny-Turner spectrometer. The instrument was equipped with a 2400 l/mm grating and a cryogenically cooled charge-coupled detector (CCD) camera (2000 × 800 pixels). The CCD detector area was read out in eight stripes stretching along the dispersion direction. The so defined regions were binned perpendicularly to the dispersion direction to reduce readout noises. The spectral dispersion of each region was calibrated separately.

The wavelength calibration was carried out with an iron hollow-cathode lamp, which emits suitably narrow lines of both the discharge gas, Ne, and the cathode material, Fe. About ten lines with interferometrically established wavelengths taken from the NIST database [15] were recorded in each calibration spectrum, with exposure times of a few minutes. These lines were then fitted with Gaussian functions to determine their positions. Their wavelength reference values were plotted versus the peak pixel position, and the resulting (almost linear) curve was fitted to a

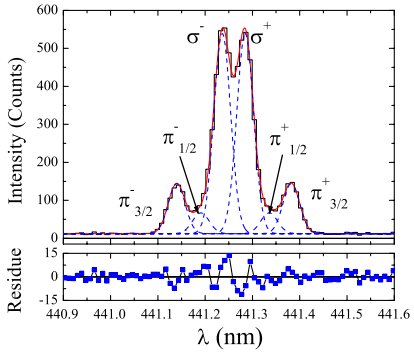

FIG. 1 (color online). A typical spectral line obtained from the $1s^2 2s^2 2p\ ^2P_{1/2} - {}^2P_{3/2}$ transition in B-like $^{40}Ar^{13+}$. The six dashed curves represent a fit to the Zeeman components.

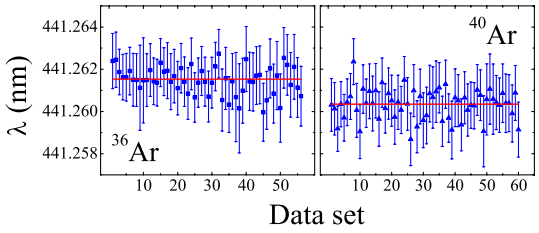

FIG. 2 (color online). Wavelengths of the σ components of the $1s^2 2s^2 2p\ {}^2P_{1/2} - {}^2P_{3/2}$ transition obtained in B-like $^{36}Ar^{13+}$ (left) and $^{40}Ar^{13+}$ (right) ions for a given CCD region (see text). The horizontal lines represent the statistically weighted average values.

parabola to obtain the instrument dispersion. Individual calibrations were carried out before and after each measurement of the Ar lines, in order to reduce the effect of possible long term shifts of the setup. The calibration lines displayed a FWHM of only a few pixels. In order to avoid sampling errors of their individual line profiles and to minimize the statistical uncertainty, 15–30 spectra of 30–50 minutes each were recorded for every line together with their corresponding calibration spectra, while gradually shifting the grating by a small angle between consecutive measurements. In this way, each CCD pixel can be viewed as an exit slit sampling the line profile in very small angular steps of the grating rotation.

In the B-like Ar measurement, we obtained two wavelength values, one from the outer $\pi_{3/2}$ components and the other from the central σ components, as shown in Fig. 1. The $\pi_{1/2}$ components could not be used since they were not completely resolved. For the Be-like line, the Zeeman splitting into 9 components was not fully resolved due to the width of the recorded lines, which was the consequence of a higher ion temperature and of the use of a wider entrance slit to compensate for the lower intensity of this line. In this case, a single Gaussian function was fitted to the experimental spectra and, thus, only one set of data was obtained for each isotope. Altogether, 30–60 independent wavelength data points were obtained for each isotope, with a remarkable reproducibility shown in Figs. 2 and 3. In the case of B-like Ar, the experimental wavelengths obtained in the present work improve the results of our earlier measurement in Ref. [12] (see also Table II below).

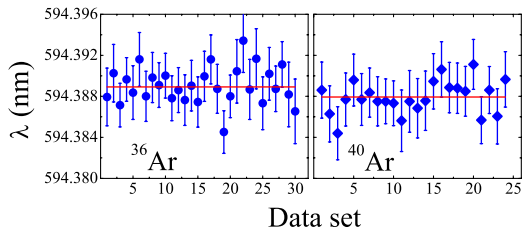

FIG. 3 (color online). Wavelengths of the $1s^2 2s2p\ {}^3P_1 - {}^3P_2$ transition obtained in Be-like $^{36}Ar^{14+}$ (left) and $^{40}Ar^{14+}$ (right) ions for a given CCD region (see text). The horizontal lines represent the statistically weighted average values.

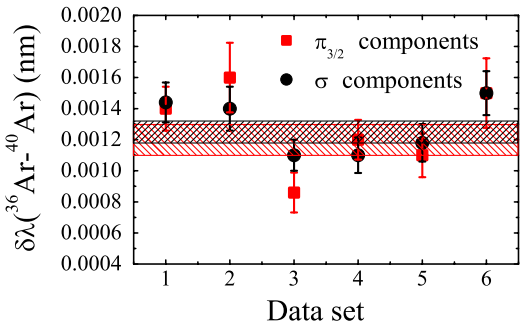

FIG. 4 (color online). Isotope effect in B-like Ar for data sets corresponding to different CCD regions (see text). The lower shadowed band (red) represents the resulting average and its error for the $\pi_{3/2}$ components and the upper shadowed band (black) the weighted average and its error obtained for the σ components.

The resulting isotope shifts in B- and Be-like Ar ions obtained from the wavelength differences in different CCD camera regions are shown in Figs. 4 and 5, respectively.

Theoretical transition energies and their isotope shifts, including the contributions due to the total recoil operator in Eq. (1), have been calculated by large-scale configuration interaction Dirac-Fock (CI-DF) calculations. The atomic state function with a given angular momentum J and parity P was expanded in terms of configuration state functions (CSFs) with the same quantum numbers J and P. Orbital functions for the occupied $1s$, $2s$, and $2p$ subshells were optimized by the DF method and virtual orbitals were generated by solving the Dirac-Fock-Sturmian equations [9]. The set of CSFs was obtained using the restricted active space method with single, double, and triple excitations. Negative spectrum contributions to the mass shift were evaluated by means of perturbation theory using the Sturmian basis. The mass shift contributions to the states under study are given in Table I. The NMS and SMS nonrelativistic operator contributions were also calculated in the framework of the multiconfiguration DF method with independent coding [16] to provide a numerical test.

The calculation of the QED contributions to the recoil effect is based on the works [11]. These corrections are

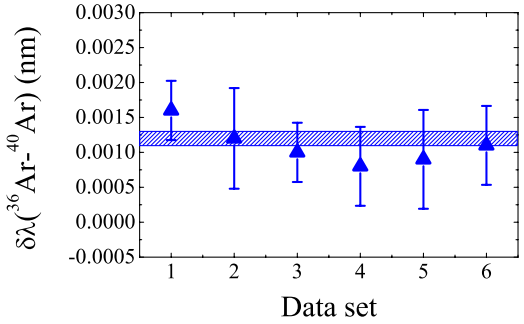

FIG. 5 (color online). Isotope effect in Be-like Ar for data sets corresponding to different CCD regions (see text). The shadowed area indicates the weighted average value and its error bar.

TABLE II. Transition wavelengths for $^{40}Ar^{13+,14+}$ and isotope shifts (^{36}Ar–^{40}Ar) (in nm, air). The π components are marked by an asterisk ($*$), σ components by a double asterisk ($**$), and their average by the superscript av. See text for further explanations.

	Wavelength (^{40}Ar)		Isotope shift (^{36}Ar–^{40}Ar)	
Ion	Theory	Experiment	Theory	Experiment
Ar^{13+}	441.16(27)	441.2556(1)	0.00123(5)	$0.00120(10)^{*}$ $0.00125(7)^{**}$ $0.00123(6)^{av}$
Ar^{14+}	594.24(30)	594.3879(2)	0.00122(5)	0.00120(10)

given in the third and sixth rows of Table I. One-electron wave functions for these calculations were obtained by solution of the Dirac equation with a localized DF potential, reproducing the $2p$ one-electron energies on the level of DF calculations or better.

The final experimental and theoretical results for the transition wavelengths in Ar^{13+} and Ar^{14+} and their respective isotope shifts are summarized in Table II. In contrast to the results of relativistic many-body perturbation theory calculations [17], the present theoretical wavelengths agree well with the experimental data. However, due to uncalculated terms, the theoretical uncertainties are 3 orders of magnitude larger than the corresponding experimental errors.

Theoretical isotope shifts including relativistic normal and specific mass shift contributions show an excellent agreement with the measured results, confirming the relativistic theory of recoil effects in many-body systems [9]. The substantially higher precision of the predicted isotope shifts in comparison with that of transition energies is due to large cancellation of terms that are virtually identical for both isotopes.

In conclusion, isotope shifts of the ground state $M1$ lines in highly charged Ar ions have been determined with high precision. The combination of the EBIT, providing a stable population of trapped HCI, with accurate calibration techniques was essential to the success of this study. A comparison to accurate calculations and a detailed theoretical analysis of the contributing effects (NMS + RNMS, SMS + RSMS) shows that it is indispensable to consider the relativistic recoil operator when predicting relativistic mass shift contributions even in medium-Z ions (see Table I). To the best of our knowledge, the relativistic nuclear recoil effect has never been observed experimentally in HCI thus far. We reemphasize that a calculation with the nonrelativistic recoil operator would give values for the mass shift which are smaller than the correct relativistic result by a factor of roughly two (Ar^{13+}) or even three (Ar^{14+}), as is evident from Table I. This demonstrates the crucial importance of using the total relativistic recoil operator in these calculations.

As a last remark, we would like to expand on the role of QED effects on the nuclear recoil in addition to the relativistic corrections: as the former are 2 orders of magnitude smaller than the total isotope shift (see Table I), their observation would require a further substantial improvement of existing experimental techniques. This could be achieved, e.g., by applying laser spectroscopic methods to trapped HCI. Because these QED contributions (beyond the Breit approximation) scale with high powers of Z, they may be observable in high-Z ions where they are comparable in size to the contributions of the relativistic recoil operator [11].

A. N. A. acknowledges support from the "Dynasty" foundation and V. M. S. and I. I. T. from the Russian Foundation for Basic Research (Grants No. N 04-02-17574 and No. N 05-03-32585). U. D. J. acknowledges support from the Deutsche Forschungsgemeinschaft (Heisenberg program).

[1] J. C. Berengut, V. A. Dzuba, and V. V. Flambaum, Phys. Rev. A **68**, 022502 (2003).
[2] E. J. Salumbides, J. P. Sprengers, E. Reinhold, and W. Ubachs, J. Phys. B **38**, L383 (2005).
[3] S. C. Bennett and C. E. Wieman, Phys. Rev. Lett. **82**, 2484 (1999).
[4] M. A. Bouchiat and C. Bouchiat, Rep. Prog. Phys. **60**, 1351 (1997).
[5] V. M. Shabaev, Teor. Mat. Fiz. **63**, 394 (1985) [Theor. Math. Phys. (Engl. Transl.) **63**, 588 (1985)]; Yad. Fiz. **47**, 107 (1988) [Sov. J. Nucl. Phys. **47**, 69 (1988)].
[6] L.-B. Wang, P. Mueller, K. Bailey, G. W. F. Drake, J. P. Greene, D. Henderson, R. J. Holt, R. V. F. Janssens, C. L. Jiang, and Z.-T. Lu *et al.*, Phys. Rev. Lett. **93**, 142501 (2004).
[7] G. Ewald, W. Nörtershäuser, A. Dax, S. Götte, R. Kirchner, H.-J. Kluge, T. Kühl, R. Sanchez, A. Wojtaszek, and B. A. Bushaw *et al.*, Phys. Rev. Lett. **93**, 113002 (2004).
[8] C. Froese Fischer, P. Jönsson, and M. Godefroid, Phys. Rev. A **57**, 1753 (1998).
[9] I. I. Tupitsyn, V. M. Shabaev, J. R. Crespo López-Urrutia, I. Draganić, R. Soria Orts, and J. Ullrich, Phys. Rev. A **68**, 022511 (2003).
[10] C. W. Palmer, J. Phys. B **20**, 5987 (1987).
[11] A. N. Artemyev, V. M. Shabaev, and V. A. Yerokhin, Phys. Rev. A **52**, 1884 (1995); J. Phys. B **28**, 5201 (1995).
[12] I. Draganić, J. R. Crespo López-Urrutia, R. DuBois, S. Fritzsche, V. M. Shabaev, R. Soria Orts, I. I. Tupitsyn, Y. Zou, and J. Ullrich, Phys. Rev. Lett. **91**, 183001 (2003).
[13] J. R. Crespo López-Urrutia, B. Bapat, I. Draganić, A. Werdich, and J. Ullrich, Phys. Scr. **T92**, 110 (2001).
[14] A. Lapierre, U. D. Jentschura, J. R. Crespo López-Urrutia, J. Braun, G. Brenner, H. Bruhns, D. Fischer, A. J. González Martínez, Z. Harman, and W. R. Johnson *et al.*, Phys. Rev. Lett. **95**, 183001 (2005).
[15] See the URL http://physics.nist.gov.
[16] F. A. Parpia, C. Froese Fischer, and I. P. Grant, Comput. Phys. Commun. **94**, 249 (1996).
[17] M. S. Safronova, W. R. Johnson, and U. I. Safronova, Phys. Rev. A **53**, 4036 (1996); Phys. Rev. A **54**, 2850 (1996).